



The geometry of sea-level change across a mid-Pliocene glacial cycle

Meghan E. King^{1*}, Jessica R. Creveling¹, Jerry X. Mitrovica²

¹College of Earth, Ocean, and Atmospheric Sciences, Oregon State University, Corvallis, OR 97331, USA

²Department of Earth and Planetary Sciences, Harvard University, Cambridge, MA 02138, USA

5 *Currently at Department of Earth and Space Sciences, University of Washington, Seattle, WA 98195, USA

Correspondence to: Meghan E. King (mking5@uw.edu)

Abstract. Predictions for future sea-level change and ice sheet stability rely on accurate reconstructions of sea level during past warm intervals, such as the mid-Pliocene Warm Period (MPWP; 3.264 – 3.025 Ma). The magnitude of MPWP glacial cycles, and the relative contribution of meltwater sources, remains uncertain. We explore this issue by modeling glacial isostatic adjustment processes for a wide range of possible MPWP ice sheet melt zones, including North America, Greenland, Eurasia, West Antarctica, and the Wilkes Basin, Aurora Basin, and Prydz Bay Embayment in East Antarctica. As a case study, we use a series of ice histories together with a suite of viscoelastic Earth models to predict global changes in sea level from the Marine Isotope Stage (MIS) M2 glacial to the MIS 15 KM3 interglacial. Our results indicate that, of the locations with stratigraphic constraints on Pliocene glacial–interglacial sea level amplitude, local sea-level (LSL) rise at Whanganui Basin, New Zealand, will be lower than the associated global mean sea level (GMSL) contribution from individual ice sheets by an average of ~20%. In contrast, LSL rise at Enewetak Atoll is systematically larger than GMSL by 10%. While no single observation (field site) can provide a unique constraint on the sources of ice melt during this period, combinations of observations 20 have the potential to yield a stronger constraint on GMSL and to narrow the list of possible sources.



1 Introduction

Accurate reconstructions of sea level during past warm periods offer insight into ice sheet stability in the face of
25 projected anthropogenic climate change (Dutton et al., 2015). In this regard, the mid-Pliocene Warm Period
(MPWP; 3.264 – 3.025 Ma) serves as a key period of focus. Mid-Pliocene reconstructed atmospheric CO₂ and
global mean annual surface temperatures are comparable to projected 21st century warming scenarios (350- 450 ppm
and ~2-3°C above modern, respectively; Pagani et al., 2010; Haywood et al., 2013) and, as such, estimates of
Pliocene peak global mean sea level (GMSL) have calibrated the sensitivity of global climate models (Deconto and
30 Pollard, 2016). While the differing rates of CO₂ forcing, and the distinct oceanographic conditions from the closing
of equatorial seaways (Haywood et al., 2011; Sarnthein et al., 2009), may reveal the MPWP as an imperfect
analogue for the future, the mid-Pliocene remains a crucial natural laboratory for evaluating the complexity of
Earth's ice age climate system.

35 A rich literature has sought to quantify GMSL variability during the MPWP using ice sheet modeling (DeConto and
Pollard, 2016; de Boer et al., 2017; Berends et al., 2019) and a suite of proxy data, including $\delta^{18}\text{O}$ records, with and
without complementary Mg/Ca measurements (e.g., Dwyer & Chandler, 2009; Sosdian & Rosenthal, 2009; Rohling
et al., 2014; Winnick and Caves, 2015; Miller et al., 2020), phreatic overgrowths on speleothems (Dumitru et al.,
2019), sequence stratigraphic records (e.g., Wardlaw and Quinn, 1991; Naish and Wilson, 2009; Miller et al., 2012;
40 Grant et al., 2019) and coastal plain terraces and escarpments (e.g., Dowsett and Cronin, 1990; Krantz, 1991;
Kaufman and Brigham-Grette, 1993; James et al., 2006; Rowley et al., 2013; Rovere et al., 2014; Hearty et al.,
2020; Sandstrom et al., 2021). These studies have evaluated both the total amplitude of sea-level change through
Pliocene glacial–interglacial cycles and the absolute peak in sea level during the Pliocene ‘super-interglacials’, yet
have achieved little consensus on these values. It is common within these studies to infer the suite of ice sheet
45 sources of meltwater on the basis of estimates of peak GMSL value (e.g., Naish and Wilson, 2009; Raymo et al.,
2011; Miller et al., 2012; Grant et al., 2019); for example, many studies attribute GMSL of up to approximately +10
m relative to present day to the combined melt from the Greenland and West Antarctic Ice Sheets, and any residual
GMSL value (i.e., > 10 m above present sea level), to meltwater from the East Antarctic Ice Sheet. More recent
studies have included North American and Eurasian ice cover in the sea level budget (Berends et al., 2019; LeBlanc
50 et al., 2021).

The persistent disagreement among the various mid-Pliocene sea-level reconstructions may stem from limitations of
the proxy records that they are derived from, or corrections applied to these proxies. Although $\delta^{18}\text{O}$ records
accurately reflect glacial time scales (Lisiecki and Raymo, 2005a; Zachos et al., 2001), numerous complexities
55 introduce errors in the mapping of these records to GMSL (Mix, 1987; Clarke and Marshall, 2002; Waelbroeck et
al., 2002; Siddall et al., 2008; Winnick and Caves, 2015). Coupled climate-ice-sea level models rely on accurate
proxy measurements and are sensitive to uncertainties in a wide range of model parameters as well as climate
forcings (e.g., Berends et al., 2019). Furthermore, an inference of local relative sea level (RSL) based on a
geomorphic or stratigraphic indicators of paleo-sea level is potentially contaminated by three geophysical



60 processes—tectonics, dynamic topography, and glacial isostatic adjustment (GIA; Raymo et al., 2011; Rowley et al., 2013; Austermann et al., 2017; Richards et al., 2023). Because each process introduces significant geographic variability to sea-level change (i.e., major regional departures from GMSL), any GMSL inference from compilations of geological data are subject to uncertainty and/or error in these geophysical corrections.

65 In this article, we explore in detail the geometries of MPWP sea-level change arising from the rotational, gravitational, and deformational effects of the GIA process for a wide range of ice sheet melt zones, including North America, Greenland, Eurasia, West Antarctica, and the Wilkes Basin, Aurora Basin, and Prydz Bay Embayment in East Antarctica. Our focus is on the geometry of sea-level change spanning from the Marine Isotope Stage (MIS) M2 glacial maximum at 3.295 Ma to the MIS KM3 interglacial at 3.155 Ma, which represent times of peak sea level
70 low and high stand, respectively. These modeling experiments complement the common focus of constraining peak sea level during the KM3 interglacial. We first describe the numerical methods adopted in the study, and the ice history and Earth models that enable sea level predictions. Next, our procedure for normalizing predictions of sea-level change requires a precise definition of GMSL change, and we discuss the definition that we adopted based on Pan et al. (2022) which, although framed for interglacials, has relevance to the discussion of Pliocene sea-level
75 change. Finally, we present and compare normalized maps of sea-level change for the individual melt zones listed above and discuss the biases in estimates of Pliocene GMSL change that may be introduced by neglecting the geographic variability inherent to these maps. We contextualize these biases for three continental shelf and upper slope environments that serve as important inferences of mid-Pliocene sea level: Virginia, United States of America (Miller et al., 2012); Enewetak Atoll, Republic of the Marshall Islands (Miller et al., 2012); and Whanganui Basin,
80 New Zealand (Naish and Wilson, 2009; Miller et al., 2012; Grant et al., 2019).

2 Methods

2.1 Sea Level Model

Our predictions are based on a generalized form of the sea-level equation (Mitrovica and Milne, 2003; Kendall et al., 2005) that accounts for time-varying shoreline migration and perturbations in Earth's rotation (Mitrovica et al.,
85 al., 2005). We assume a spherically symmetric, Maxwell viscoelastic Earth (Peltier, 1974) and adopt the pseudo-spectral algorithm described by Kendall et al. (2005) with a truncation at spherical harmonic degree and order 256. The elastic structure of the Earth model is taken from the seismic model PREM (Dziewonski and Anderson, 1981) and, in our primary calculations, the viscosity structure is comprised of a 96-km-thick elastic lithosphere and
90 uniform upper and lower mantle viscosity of 5×10^{20} Pa s and 5×10^{21} Pa s, respectively (henceforth, the 'reference' model). This primary viscoelastic structure is within the range of models inferred from studies of GIA datasets (Mitrovica and Forte, 2004; Lambeck et al., 2014), however, we also perform an analysis that explores the sensitivity of the normalized sea level predictions to plausible variations in the viscosity model.

95 Definitions of how GMSL changes through a deglaciation (or a glaciation) are complicated by contemporaneous changes in ocean area (i.e., shoreline migration) due to local onlap or offlap of water and the advance or retreat of



grounded, marine based ice sheets. Figure 1 is a schematic of the definition adopted in this study. The figure shows a cross section through a region with a grounded, marine-based ice sheet that retreats, leading to perturbations in the elevations of the solid Earth and the equipotential that defines the sea surface. We followed Pan et al. (2022) in
100 defining GMSL change from MIS M2 to KM3 as the mean change in the volume of the ocean outside the grounding line of the ice sheet prior to the melt event (i.e., to the left of the vertical dashed line marked GL on Fig. 1a) divided by the average of ocean area at the beginning and end of the time period of interest (Figs. 1a and b, respectively). (We note that in the simulations we discuss below, the ocean areas at MIS M2 and MIS KM3 differ by less than
105 ~1%, and so choosing to divide by the ocean area at either time instead of taking the average would have a negligible impact on the normalization procedure.) This definition, henceforth $GMSL_P$, reflects our focus on sea-level changes outside marine-based sectors. A more standard definition of the GMSL change, $GMSL_S$, would be to take the total volume of meltwater and divide by the average ocean area. This definition is less appropriate since it does not account for the meltwater sequestered in marine regions exposed by the retreat of grounded ice and the flux out of these areas due to post-glacial rebound. While we present both values for comparison (Table 1), in this study
110 we normalize predictions of the sea-level change from MIS M2 to KM3 by dividing each prediction by the $GMSL_P$ change associated with the GIA simulation.

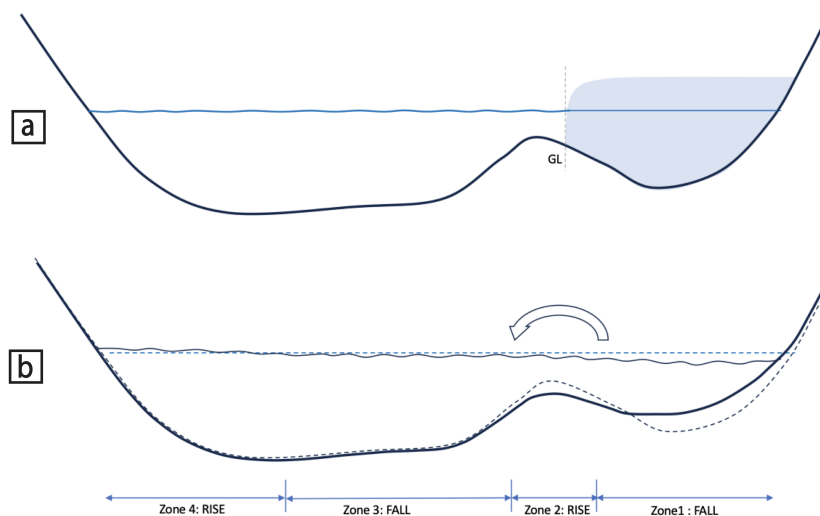


Figure 1. Sea-level change in response to the melting of a grounded ice sheet. Sea surface equipotential (blue) and solid surface (black) before (a) and after (b) the melt event. Labeling at bottom of (a) denotes the ice sheet grounding line (GL), and (b) indicates locations where sea-level rise (an increase in the elevation of sea surface equipotential relative to the solid surface) or fall (elevation of sea surface equipotential relative to solid surface decreases). Zones 1-4 are referred to in the text. The arrow at the top of frame (b) indicates the flow of water into the open ocean driven by the post-glacial uplift of marine sectors previously covered by grounded ice.

120

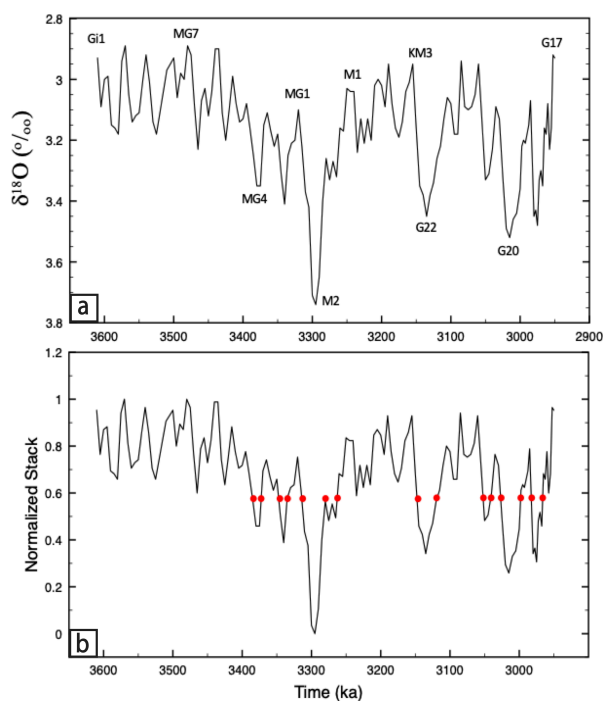


125 **Table 1. Computed GMSL changes across the ~100 kyr time period extending from MIS M2 to MIS KM3 for eight regional ice histories.** First two columns; GMSL_P (calculated using the reference earth model) and GMSL_S. The two definitions of GMSL are defined in the text. Last three columns; predicted LSL changes (in meters) and normalized sea-level change at three sites (Enewetak Atoll, Whanganui Basin and Virginia).

Ice History	GMSL _P (m)	GMSL _S (m)	Enewetak Atoll		Whanganui Basin		Virginia	
			LSL (m)	Normalized	LSL (m)	Normalized	LSL (m)	Normalized
North America	33.12	34.03	35.8	1.08	29.04	0.88	15.90	0.48
Greenland	6.67	6.75	7.29	1.09	5.25	0.79	4.80	0.72
Eurasia	4.23	4.83	4.55	1.08	3.32	0.78	3.98	0.94
East Antarctica	11.08	13.64	12.2	1.10	9.31	0.84	9.31	0.84
West Antarctica	2.74	4.87	2.78	1.01	2.39	0.87	2.77	1.01
Aurora Basin	6.72	7.64	7.35	1.09	5.24	0.78	5.04	0.75
Wilkes Basin	4.87	5.6	5.3	1.09	3.37	0.69	3.85	0.79
Prydz Bay	1.92	2.24	2	1.04	1.78	0.93	1.56	0.81

2.2 Ice Sheet Model

130 To explore the GMSL_P change in response to the collapse of an individual Pliocene ice sheet we separately modeled ice sheet variability across eight different regions during the MPWP: Eurasia (EIS), Greenland (GrIS), North America (NAIS), West Antarctica (WAIS), East Antarctica (EAIS) as well as three distinct zones within East Antarctica, including the Aurora and Wilkes Basins and Prydz Bay. Before any computation was performed, we began by establishing the maximum ice cover of individual ice sheets (GMSL_S for each is listed in Table 1). The maximum ice volume for each ice sheet occurs at MIS M2 ($\delta^{18}\text{O}$ value of 3.74 in Fig. 2a), whereas the minimum occurs at MIS MG7 (peak-interglacial sea level during our modeled time period; $\delta^{18}\text{O}$ value of 3.89 in Fig. 2a).



140 **Figure 2. Time series used in model simulations.** (a) LR04 (Lisiecki and Raymo, 2005) $\delta^{18}\text{O}$ isotopic stack extending from 3610 ka to 2950 ka with labeled Marine Isotope Stage names. (b) Normalized version of the time series in (a), constructed as described in the main text. All points on the time series with the same normalized value have an identical ice geometry (e.g., red points represent those times with a normalized value of 0.6 with precisely the same ice geometry).

Next we adopted a series of Pliocene-realistic ice geometries from the hybrid ice sheet-climate model results of
145 Berends et al. (2019). These included snapshots of EIS, GrIS, NAIS and Antarctica at MIS M2 and KM3 (Fig. 3), as well as ~25 snapshots at several intervening sea level equivalent (SLE) ice volumes. Where the maximum M2 SLE ice volume (Table 1) was greater than the Berends et al. (2019) output (e.g., ~34 m SLE from NAIS), additional snapshots with larger ice volumes were supplemented from Berends et al. (2018; e.g., Last Glacial Maximum). The Antarctica ice geometries were first split along the Transantarctic Mountains to produce separate EAIS and WAIS
150 geometries. The EAIS geometries were further broken down by underlying topography to delineate the Aurora Basin, Wilkes Basin and Prydz Bay sub-regions. Additionally, at the MIS MG7 sea-level highstand all ice sheets, with the exception of EAIS, are entirely deglaciated. For EAIS, whose peak-interglacial melting only involved the marine-based portion, the land-based EAIS (~47 m SLE) always remained during model interglacials (geometry based on the ‘PRISM’ ice-sheet configuration from Dowsett et al., 2010).

155

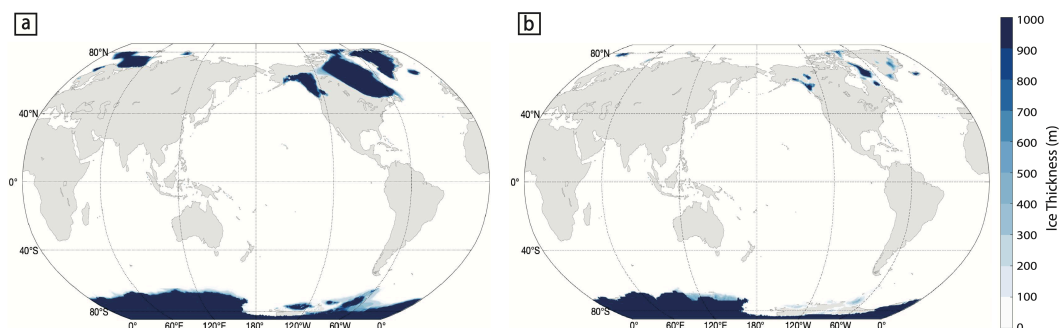


Figure 3. Modeled Pliocene ice cover during (a) MIS M2 and (b) MIS KM3. Geometries are based on the hybrid ice sheet-climate model outputs of Berends et al. (2019) as described in the text. Note that in this study each region was modeled separately, but the ice sheet extents were combined in this figure for brevity.

160

We next used the Lisiecki and Raymo (2005) benthic oxygen isotope stack (Fig. 2a) to model the time variation of ice volumes from ~300 kyr prior to MIS M2 (i.e., ~3.6 Ma) to ~200 kyr after MIS KM3 (2.95 Ma). (Ice-volume changes prior to this period would not impact predictions of sea-level change between MIS M2 and KM3.)

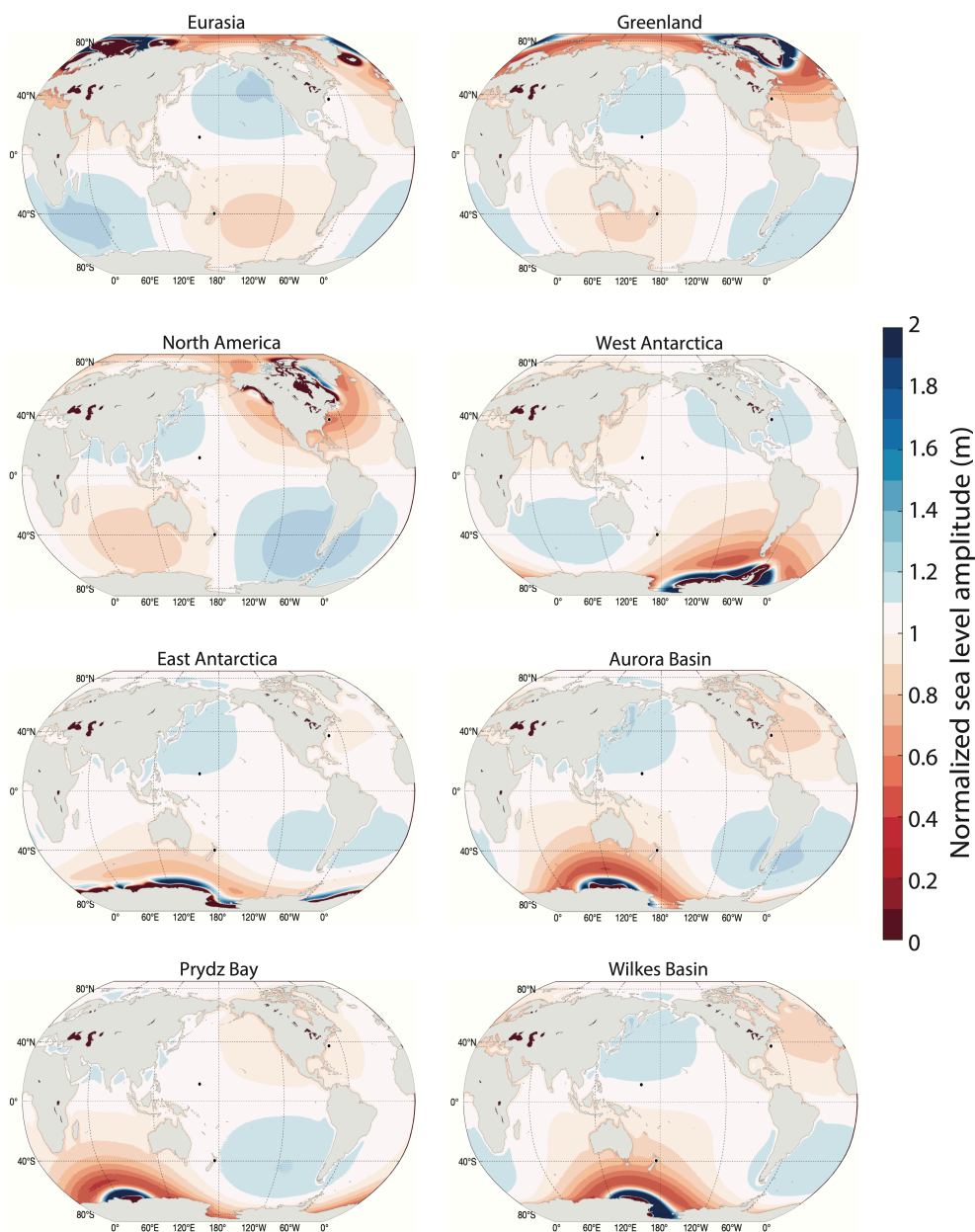
Specifically, we normalized the magnitude of isotopic variation across this interval to a scale of 0.0–1.0 by subtracting the most depleted $\delta^{18}\text{O}$ value (2.89‰ at MIS MG7) from the interval between ~3.6 and 2.9 Ma, then dividing the result by the maximum residual $\delta^{18}\text{O}$ value corresponding with the MIS M2 glaciation (3.74–2.89 = 0.85‰), and, finally, subtracting the resulting value from 1.0. This normalized time series is shown in Fig. 2b. The SLE ice volumes intermediate between the maximum (MIS M2) and minimum (MIS MG7) glacial conditions in Fig. 3 are assumed to scale linearly with the normalized $\delta^{18}\text{O}$ time-series and ice geometries are smoothly interpolated across time steps of 1 kyr to accomplish this variation. The construction is performed under the additional constraint that the ice geometry is always the same for the same normalized $\delta^{18}\text{O}$ value (e.g., the model ice geometries are identical at each of the times indicated by the red dots on Fig. 2b).

170

3 Results

Figure 4 shows maps of sea-level change computed for the eight different regional ice histories normalized by the GMSL_p change associated with each ice history (Table 1). These plots can be interpreted as ‘viscoelastic’ fingerprints that include both the viscous and elastic effects through the MIS M2 – KM3 period. (The term ‘viscoelastic’ fingerprint is used to distinguish the maps from commonly published ‘elastic’ fingerprints which are computed for melt events sufficiently rapid that viscous effects can be ignored).

175



180

Figure 4. Predicted sea-level change from MIS M2 to MIS KM3 for eight different regional ice histories (as labeled). Predictions are based on the reference viscoelastic Earth model described in the text and, to facilitate comparison, are normalized by the $GMSL_P$ change associated with each simulation (Table 1). The three black dots on the figure show the location of continental shelf/upper slope sites discussed in the text.

185



As noted, Table 1 also shows GMSL change (in meters) computed for each ice history using the definition GMSLs described above. The limitation of adopting this definition is most pronounced in the results for West Antarctica, where substantial marine-based regions are exposed across the ice history. The difference in the GMSL calculations (4.87 - 2.74 ~ 2.13 m) largely reflects the volume of meltwater that remains in these marine-based sectors at MIS 190 KM3 that were exposed by grounded ice retreat from MIS M2 to KM3.

The normalized maps in Fig. 4 show similar structures in relation to the zones of ice mass flux. In the area once covered by ice, a sea-level fall of high magnitude (off the scale of the plot) is predicted and as one considers sites progressively further from this region, zones of sea-level rise (blue, which also reaches amplitudes off scale) and fall 195 (light to dark red) are predicted. Superimposed on these trends is a so-called “quadrantal” (spherical harmonic degree two, order one) sea level pattern due to true polar wander (TPW; Milne and Mitrovica, 1996). TPW contributes a sea-level fall in the quadrant encompassing ice melt and in the anti-polar quadrant, and a sea-level rise in the remaining two quadrants. As an example, melting over Laurentia contributes a TPW-induced sea-level fall over North America and the southern Indian Ocean and a sea-level rise centered over southern South America and 200 southeast Asia.

Putting aside the TPW signal, the origin of the complex trends in the predicted sea-level change as one moves from the near to far field of an ice sheet (Fig. 4), which are characterized by several changes in sign, is captured in the schematic of Fig. 1. The total change in sea level can be understood as having two contributions. First, a reduction 205 in the ice mass from MIS M2 to KM3 leads to a migration of water from the near to far field as the gravitational pull of the ice sheet weakens. This leads to a long wavelength tilting of the sea surface up-toward-the-far field on Fig. 1b (blue wavy line). Second, superimposed on this gravitational signal, is viscous deformation comprised of post-glacial rebound in the zone of ice retreat (zone labeled 1), subsidence of a peripheral bulge (zone 2), and relatively minor crustal subsidence due to ocean loading (zone 3). In zone 1, post-glacial rebound and the loss of gravitational 210 pull on the ocean combine constructively to produce a sea-level fall with a peak amplitude more than 10 times greater than the GMSL rise of the ice history (red, largely covered by the continental mask used on the figures). In zone 2, peripheral subsidence is of greater magnitude than the water migration away from the near field and the result is a predicted sea-level rise in the maps of Figure 4 (blue contours). In zone 3, the opposite happens; the long wavelength tilting of the sea-surface (and migration of water) due to the loss of gravitational pull toward the ice 215 sheet once again dominates crustal subsidence and a sea-level fall is predicted (red zone encircling the blue). In zone 3 the predicted sea-level fall also has a contribution from ocean syphoning, the movement of water away from these regions into the accommodation created primarily by the subsiding peripheral bulges (Mitrovica and Milne, 2002). Finally, water migration into zone 4 dominates other effects and sea level rise occurs.

220 The viscoelastic fingerprint maps in Fig. 4 highlight the significant departures from GMSL for the period extending from MIS M2 glacial maximum to MIS KM3 glacial minimum. The geographic pattern of these departures is governed by the location of the modeled ice melt. We next turn to the implications of this variability on inferences



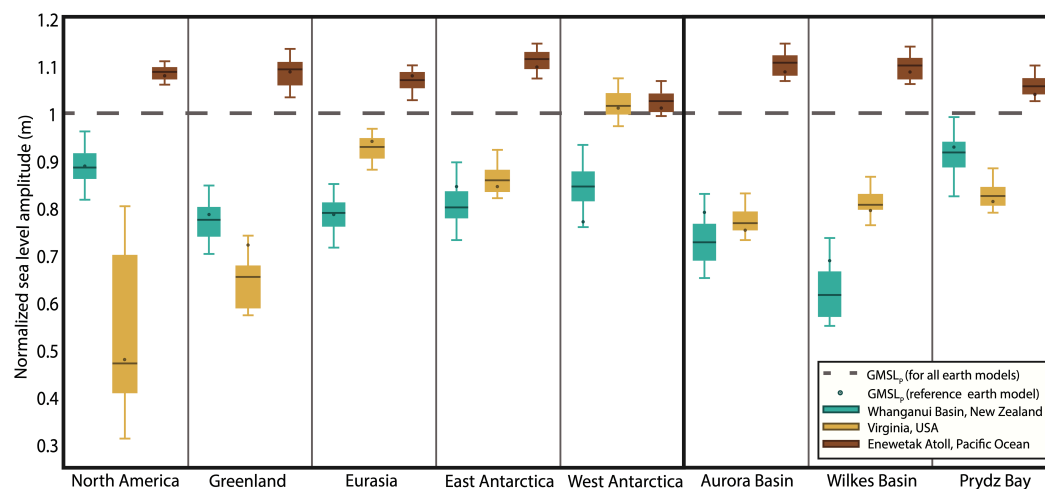
of the total amplitude of GMSL change inferred from geological indicators of sea-level change across the super glacial-interglacial cycle.

225

To assess the sensitivity of MPWP GMSL to the adopted Earth model, we ran 24 additional simulations in which the lithospheric thickness varied from 72-125 km, upper mantle viscosity from $2-8 \times 10^{20}$ Pa s, and lower mantle viscosity from $5-30 \times 10^{21}$ Pa s. Figure 5 shows, for all eight regional ice histories, the full range of normalized sea level predictions for all 24 earth models at the three representative geographic localities that host intensively studied MPWP stratigraphic indicators—one in the near field of Northern Hemisphere ice sheets (Virginia), one in the near field of Antarctica (Whanganui Basin), and one in the far field of all ice sheets (Enewetak Atoll). The range of predictions, each normalized by the $GMSL_P$ of the scenario (as defined in the discussion of Fig. 1; Pan et al., 2021), is summarized by a box and whiskers plot (Fig. 5). The black circle within the box and whisker plot refers to the value of sea-level change for the reference earth model and individual ice sheet, while the black line demonstrates the median value for all 24 earth models for an individual ice sheet. The normalization procedure allows us to meaningfully compare the results across these models. Therefore, values above $GMSL_P = 1$ refer to local predictions of sea-level change greater than the global mean, whereas values below $GMSL_P = 1$ refer to predictions less than the global mean.

230

235



240

Figure 5. Predicted MIS M2 to MIS KM3 sea-level changes for three geographic sites (see inset key, and Fig. 4 for locations) based upon a range of melt and viscoelastic Earth models. The box-and-whisker plots show the range of results generated using the 24 different viscoelastic models (discussed in the text). All predictions are normalized by the global mean, $GMSL_P$, associated with the specific melt and Earth models. The dashed line denotes the result that would occur if the prediction matched the associated $GMSL_P$ value and, thus, departures from 1.0 represent normalized (fractional) departures from the global mean change in sea level as defined by Pan et al. (2021).

245

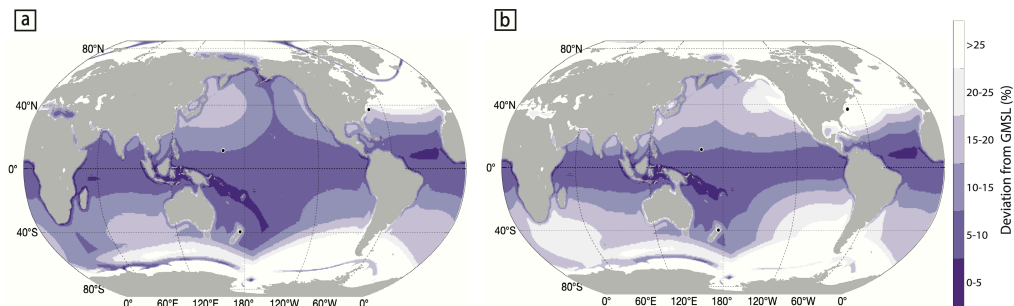
Predictions at Enewetak Atoll, in the very far field of ice mass changes are consistently ~0-15% greater than $GMSL_P$ (Fig. 5). This site is within zone 4 of Fig. 1 but the prediction is influenced in some simulations by rotational effects (Fig. 4). The predictions of sea-level change at Whanganui Basin have a larger spread than those for

250



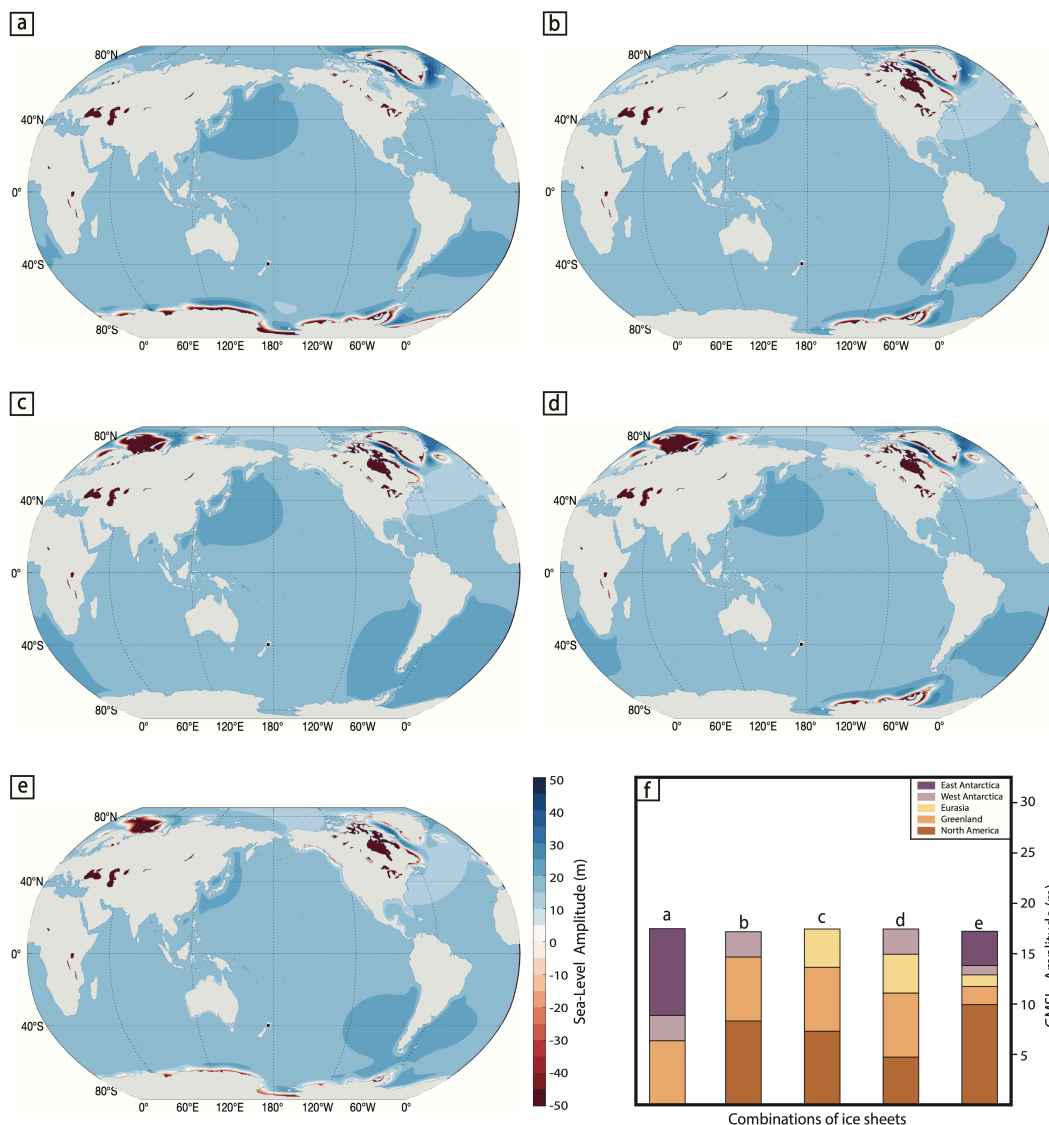
Enewetak and are consistently below the global mean ($GMSL_P$) for all melt models and for all Earth models. In the case of melting in the northern hemisphere (e.g., EIS, GrIS and NAIS melt models) the departure from $GMSL_P$ is dominated by the sea-level fall associated with rotational effects (Fig. 4). These effects also contribute to the results
255 for southern hemisphere melt models, but in those cases the migration of water away from the zones of melt tends to dominate (Fig. 1; zone 3), particularly in the case of melt from the Aurora and Wilkes Basins (Figs. 4 and 5). In the case of these melt zones, the local prediction at Whanganui Basin reaches only ~60-80% of the global mean value. The predictions at Virginia, on the United States' east coast, show even greater sensitivity to the location of melt. In the case of the simulations involving melt from NAIS or GrIS, the prediction is dominated by the migration of water
260 away from the area of melt (Fig. 1; zone 3) and rotational effects, which lead to a sea-level change substantially lower than $GMSL_P$ (Fig. 5). Rotational effects dominate the departure from the global mean and contribute a sea-level fall for all cases of melt within the East Antarctic and a sea-level rise for melt sourced from West Antarctica.

To identify geographic regions in which local sea level (LSL) variation might provide the closest measure of $GMSL_P$ from MIS M2 to MIS KM3, Fig. 6 plots the maximum discrepancy from the total $GMSL_P$ computed using the reference Earth model and the following combinations of ice melt models: GrIS, WAIS, and EAIS (Fig. 6a); and NAIS, EIS, GrIS, WAIS, and marine-based EAIS (Fig. 6b). The first combination of ice melt sources reflects the view that only the modern-day ice sheets contributed melt from MIS M2 to the KM3 interglacial, whereas the second melt source combination incorporates a contribution from two additional ice sheets (NAIS and EIS) across
270 this time period. Recent studies have included NAIS and EIS contributions to the sea level budget (Berends et al., 2019; LeBlanc et al., 2021). For both scenarios, the maximum discrepancy is highest within the near field of the modeled ice mass flux (both scenarios yield discrepancies greater than 20% at Virginia) and lowest in equatorial regions in the far field. In both scenarios, areas in the equatorial Atlantic and a stretch of Pacific Ocean extending from Indonesia to Fiji are predicted to have experienced a sea-level change from MIS M2 to MIS KM3 within 5%
275 of the global mean value. In contrast, the discrepancy is large (>10%) along most of the global coastline. Additionally, at Enewetak Atoll and Whanganui Basin, the scenarios yield consistent deviations of up to 15% and 20% from $GMSL_P$, respectively (Fig. 6). (Note that for the Whanganui Basin the colored area indicating 20% is partially obscured by the land mask). In summary, Fig. 6 presents the narrow geographic areas across the Pliocene globe that could accurately approximate melt from all ice sheets. These percent discrepancies, and indeed the
280 departure from $GMSL_P$ of any other combination of melt sources, can be inferred from the individual ice sheet results in Fig. 5.



285 **Figure 6. The maximum percent discrepancy of the reference viscoelastic Earth model predictions of LSL change from GMSL_P across MIS M2 to MIS KM3.** The following scenarios of ice melt locations are commonly forwarded in published literature: (a) Greenland, West Antarctica, and marine-based East Antarctica; and (b) North America, Eurasia, Greenland, West Antarctica, and East Antarctica.

Since Whanganui Basin is the only site with a published estimate of sea-level change across the MIS M2 – KM3
290 deglaciation (Grant et al., 2019), we further explored the discrepancy between global and LSL at this site. It is clear from Fig. 5 that any inference of the LSL change at this site will always be smaller than the GMSL. Figure 7 illustrates five example scenarios where combinations of ice sheet melt, in conjunction with the reference earth model, predict a ~15 m amplitude LSL rise across this deglaciation at Whanganui Basin. Bar plots (Fig. 7f) provide the GMSL_P value from each ice sheet in a given scenario (a–e), as well as the total. This result emphasizes the
295 systematic difference between LSL change at Whanganui Basin and GMSL, and highlights the obvious non-uniqueness associated with inferring melt source(s) from a measurement at one locality. In these scenarios, LSL change at Whanganui change is consistently ~20% lower than GMSL_P.



300 **Figure 7. Catalog of ice-sheet combinations that produce 15 m amplitude LSL change at Whanganui Basin, New Zealand.**
 (a-e) Global maps of the total sea-level change from the MIS M2 glacial to the MIS KM3 interglacial for the five scenarios of ice
 sheet melt. Frame (f) shows the global mean (GMSL_p) associated with each of the 5 melt scenarios and the contribution to this
 305 value from each region of melt.

4 Discussion and Conclusions

Our analysis has highlighted the geographically variable change in sea level associated with a variety of potential meltwater sources to a major MPWP glacial–interglacial cycle. This variability provides a direct measure of the departure of local sea-level rise from the global mean anywhere in the global ocean (Fig. 4), including sites that
 310 have contributed to estimates of peak and glacial cycle sea-level change during MPWP. Discussions of this



departure require a robust and transparent definition of GMSL. Consider, for example, the five melt scenarios in Fig. 7 that each yield a LSL change of 15 m at Whanganui Basin from MIS M2 to KM3. When accounting for the meltwater sequestered in marine regions exposed by the retreat of grounded ice, these scenarios are characterized by a GMSL_P of 18.16, 17.82, 18.25, 18.24, and 17.58 m, respectively. In contrast, if we had adopted GMSL_S (Table 1), which only considers the total volume of meltwater divided by the average ocean area, the estimates of global mean would be higher: 22.40, 20.26, 19.31, 21.18, and 19.49 m, respectively. Therefore, adopting the GMSL_S calculation can overestimate the difference between local and global mean sea level, particularly when melt from the Antarctic ice sheet is involved.

315

320 The Whanganui Basin hosts well-preserved Pliocene continental shelf stratigraphy (Naish and Wilson, 2009). Assuming the modern wave climate was similar to the Pliocene, Grant et al. (2019) applied a theoretical relationship between modern sediment transport by waves and water depth to temporal variation in grain in Pliocene core/outcrop samples and then applied a two-dimensional backstripping method to correct for the effects of tectonic subsidence and sediment compaction to estimate the amplitude of MIS M2 to MIS KM3 LSL change of 13 ± 5 m.

325 Grant et al. (2019) noted that, while their analysis strictly provided a measure of *local* RSL change, their modeling of GIA indicated that the reconstruction also served as a good approximation of GMSL and, thus, ice-volume fluctuation. The results of Figs. 4–7 indicate that this local measurement will be lower than the associated GMSL_P by an average of ~20%.

330 Beyond a robust estimate of GMSL change across the MIS M2 to KM3 deglaciation, a further goal of MPWP paleo-sea level studies is to constrain the sources of ice mass flux and their relative contributions. For a given site, the greater (smaller) the spread of the box-and-whisker predictions across the various melt scenarios (Fig. 5), the greater (lower) the ability of that observation, when viewed in combination with other observations, to constrain the contributors to the sea-level change from the MIS M2 glacial to the MIS KM3 interglacial. As an example, an accurate observation at Enewetak Atoll would provide a powerful constraint on GMSL_P because all melt zones provide a consistent scale factor between LSL change and GMSL_P. Yet that consistency indicates, conversely, that this datum provides no discriminatory information on the melt source(s). Combining this observation with one at Virginia, and/or Whanganui Basin might yield both a strong constraint on GMSL_P and narrow the possible sources of melt. Further exploration of the results of Fig. 4 will provide other potential sites that can contribute to

335

340 establishing such constraints.

Code and Data Availability

Data for the ice and sea level models, as well as code used to produce figures will be available at <https://github.com/meghan-king/plioceneSeaLevel> upon publication.

345



Author Contribution

MEK, JRC and JXM designed the study and MEK performed all the simulations. MEK prepared the manuscript and
350 figures with contributions from JRC and JXM.

Competing Interests

The authors declare no competing interests with respect to the results of this paper.

355 Acknowledgements

We thank C.J. Berends for the MPWP ice snapshots.

Financial Support

This research was made possible by U.S. National Science Foundation award 2046244, a Geological Society of
360 America (GSA) graduate student research grant, and the Oregon State University George and Danielle Sharp
Fellowship.

References

- 365 Austermann, J., Mitrovica, J. X., Huybers, P., and Rovere, A.: Detection of a dynamic topography signal in last
interglacial sea-level records, *Science Advances*, 3, e1700457, <https://doi.org/10.1126/sciadv.170045>, 2017.
- Berends, C. J., De Boer, B., and Van De Wal, R. S.: Application of HadCM3@ Bristol v1.0 simulations of
paleoclimate as forcing for an ice-sheet model, ANICE2. 1: set-up and benchmark experiments, *Geoscientific
Model Development*, 11, 4657-4675, <https://doi.org/10.5194/gmd-11-4657-2018>, 2018.
370
- Berends, C. J., Boer, B. D., Dolan, A. M., Hill, D. J., and Van De Wal, R. S.: Modelling ice sheet evolution and
atmospheric CO₂ during the Late Pliocene, *Climate of the Past*, 15, 1603-1619, <https://doi.org/10.5194/cp-15-1603-2019>, 2019.
- 375 Clarke, G. K., & Marshall, S. J.: Isotopic balance of the Greenland Ice Sheet: modelled concentrations of water
isotopes from 30,000 BP to present, *Quaternary Science Reviews*, 21, 419-430,
[https://doi.org/10.1016/S0277-3791\(01\)00111-1](https://doi.org/10.1016/S0277-3791(01)00111-1), 2002.
- de Boer, B., Haywood, A. M., Dolan, A. M., Hunter, S. J., and Prescott, C. L.: The transient response of ice volume
to orbital forcing during the warm late Pliocene, *Geophysical Research Letters*, 44, 10-486,
380 <https://doi.org/10.1002/2017GL073535>, 2017.
- DeConto, R. M., and Pollard, D.: Contribution of Antarctica to past and future sea-level rise, *Nature*, 531, 591-597,
<https://doi.org/10.1038/nature17145>, 2016.
- 385 Dowsett, H. J., and Cronin, T. M. High eustatic sea level during the middle Pliocene: Evidence from the
southeastern US Atlantic Coastal Plain, *Geology*, 18, 435-438, [https://doi.org/10.1130/0091-7613\(1990\)018<0435:HESLDT>2.3.CO;2](https://doi.org/10.1130/0091-7613(1990)018<0435:HESLDT>2.3.CO;2), 1990.
- Dowsett, H., Robinson, M., Haywood, A. M., Salzmann, U., Hill, D., Sohl, L. E., ... and Stoll, D. K.: The PRISM3D
paleoenvironmental reconstruction, *Stratigraphy*, 7, 123-139, <https://doi.org/10.29041/strat.07.2.03>, 2010.
390
- Dumitru, O. A., Austermann, J., Polyak, V. J., Fornós, J. J., Asmerom, Y., Ginés, J., ... and Onac, B. P.: Constraints
on global mean sea level during Pliocene warmth, *Nature*, 574, 233-236, <https://doi.org/10.1038/s41586-019-1543-2>, 2019.
395



- Dutton, A., Carlson, A. E., Long, A. J., Milne, G. A., Clark, P. U., DeConto, R., ... and Raymo, M. E.: Sea-level rise due to polar ice-sheet mass loss during past warm periods, *Science*, 349, aaa4019, <https://doi.org/10.1126/science.aaa4019>, 2015.
- 400 Dwyer, G. S., & Chandler, M. A.: Mid-Pliocene sea level and continental ice volume based on coupled benthic Mg/Ca palaeotemperatures and oxygen isotopes, *Philosophical Transactions of the Royal Society A: Mathematical, Physical and Engineering Sciences*, 367, 157-168, <https://doi.org/10.1098/rsta.2008.02>, 2009
- 405 Dziewonski, A.M., and Anderson, D.L.: Preliminary reference Earth model: Physics of the Earth and Planetary Interiors, 25, 297–356, [https://doi.org/10.1016/0031-9201\(81\)90046-7](https://doi.org/10.1016/0031-9201(81)90046-7), 1981.
- Grant, G. R., Naish, T. R., Dunbar, G. B., Stocchi, P., Kominz, M. A., Kamp, P. J., ... and Patterson, M. O.: The amplitude and origin of sea-level variability during the Pliocene epoch, *Nature*, 574, 237-241. <https://doi.org/10.1038/s41586-019-1619-z>, 2019.
- 410 Haywood, A. M., Dowsett, H. J., Robinson, M. M., Stoll, D. K., Dolan, A. M., Lunt, D. J., ... and Chandler, M. A.: Pliocene Model Intercomparison Project (PlioMIP): experimental design and boundary conditions (experiment 2), *Geoscientific Model Development*, 4, 571-577, <https://doi.org/10.5194/gmd-4-571-2011>, 2011.
- 415 Haywood, A. M., Hill, D. J., Dolan, A. M., Otto-Blietsner, B. L., Bragg, F., Chan, W. L., ... and Zhang, Z.: Large-scale features of Pliocene climate: results from the Pliocene Model Intercomparison Project, *Climate of the Past*, 9, 191-209, <https://doi.org/10.5194/cp-9-191-2013>, 2013.
- 420 Hearty, P. J., Rovere, A., Sandstrom, M. R., O'Leary, M. J., Roberts, D., and Raymo, M. E. Pliocene-Pleistocene Stratigraphy and Sea-Level Estimates, Republic of South Africa With Implications for a 400 ppmv CO₂ World, *Paleoceanography and paleoclimatology*, 35, e2019PA003835, <https://doi.org/10.1029/2019PA003835>, 2020.
- 425 James, N. P., Bone, Y., Carter, R. M. nd Murray-Wallace, C. V.: Origin of the late Neogene Roe Plains and their calcarenite veneer: Implications for sedimentology and tectonics in the Great Australian Bight, *Aust. J. Earth Sci.*, 53, 407–419, <https://doi.org/10.1080/08120090500499289>, 2006.
- 430 Kaufman, D. S., and Brigham-Grette, J.: Aminostratigraphic correlations and paleotemperature implications, Pliocene-Pleistocene high-sea-level deposits, northwestern Alaska, *Quaternary Science Reviews*, 12, 21-33. [https://doi.org/10.1016/0277-3791\(93\)90046-O](https://doi.org/10.1016/0277-3791(93)90046-O), 1993.
- 435 Kendall, R. A., Mitrovica, J. X., and Milne, G. A.: On post-glacial sea level–II, Numerical formulation and comparative results on spherically symmetric models, *Geophysical Journal International*, 161, 679-706, <https://doi.org/10.1111/j.1365-246X.2005.02553.x>, 2005.
- Krantz, D. E.: A chronology of Pliocene sea-level fluctuations: The US Middle Atlantic Coastal Plain record, *Quaternary Science Reviews*, 10, 163-174, [https://doi.org/10.1016/0277-3791\(91\)90016-N](https://doi.org/10.1016/0277-3791(91)90016-N), 1991.
- 440 Lambeck, K., Rouby, H., Purcell, A., Sun, Y., and Sambridge, M.: Sea level and global ice volumes from the Last Glacial Maximum to the Holocene, *Proceedings of the National Academy of Sciences*, 111, 15296-15303, <https://doi.org/10.1073/pnas.1411762111>, 2014.
- 445 LeBlanc, D. E.: Cosmogenic nuclides in ocean mud inform ice sheet history, *Nature Reviews Earth & Environment*, 2, 664-664, <https://doi.org/10.1038/s43017-021-00220-5>, 2021.
- Lisiecki, L. E., and Raymo, M. E.: A Pliocene-Pleistocene stack of 57 globally distributed benthic $\delta^{18}\text{O}$ records, *Paleoceanography*, 20, <https://doi.org/10.1029/2004PA001071>, 2005.



- 450 Miller, K. G., Wright, J. D., Browning, J. V., Kulpecz, A., Kominz, M., Naish, T. R., ... and Sosdian, S: High tide of
the warm Pliocene: Implications of global sea level for Antarctic deglaciation, *Geology*, 40, 407-410,
<https://doi.org/10.1130/G32869.1>, 2012.
- 455 Miller, K. G., Browning, J. V., Schmelz, W. J., Kopp, R. E., Mountain, G. S., and Wright, J. D.: Cenozoic sea-level
and cryospheric evolution from deep-sea geochemical and continental margin records, *Science
advances*, 6(20), eaaz1346, <https://doi.org/10.1126/sciadv.aaz1346>, 2020.
- 460 Milne, G. A., and Mitrovica, J. X.: Postglacial sea-level change on a rotating Earth: first results from a
gravitationally self-consistent sea-level equation, *Geophysical Journal International*, 126, F13-F20,
<https://doi.org/10.1111/j.1365-246X.1996.tb04691.x>, 1996.
- 465 Mitrovica, J. X., and Forte, A. M.: A new inference of mantle viscosity based upon joint inversion of convection
and glacial isostatic adjustment data, *Earth and Planetary Science Letters*, 225, 177-189,
<https://doi.org/10.1016/j.epsl.2004.06.005>, 2004.
- Mitrovica, J. X., and Milne, G. A.: On the origin of Late Holocene highstands within equatorial ocean
basis, *Quaternary Science Reviews*, 21, 2179-2190, [https://doi.org/10.1016/S0277-3791\(02\)00080-X](https://doi.org/10.1016/S0277-3791(02)00080-X), 2002.
- 470 Mitrovica, J. X., and Milne, G. A.: On post-glacial sea level: I. General theory, *Geophysical Journal
International*, 154, 253-267, <https://doi.org/10.1046/j.1365-246X.2003.01942.x>, 2003.
- Mitrovica, J. X., Wahr, J., Matsuyama, I., and Paulson, A.: The rotational stability of an ice-age earth, *Geophysical
Journal International*, 161, 491-506, <https://doi.org/10.1111/j.1365-246X.2005.02609.x>, 2005.
- 475 Mix, A. C.: The oxygen-isotope record of glaciation, in: *North America and adjacent oceans during the last
deglaciation*, edited by: W. F. Ruddiman, and H. E. Wright, 111–135, <https://doi.org/10.1130/DNAG-GNA-K3.111>, 1987.
- 480 Naish, T. R., & Wilson, G. S.: Constraints on the amplitude of Mid-Pliocene (3.6–2.4 Ma) eustatic sea-level
fluctuations from the New Zealand shallow-marine sediment record, *Philosophical Transactions of the Royal
Society A: Mathematical, Physical and Engineering Sciences*, 367, 169-187,
<https://doi.org/10.1098/rsta.2008.0223>, 2009.
- 485 Pagani, M., Liu, Z., LaRiviere, J., and Ravelo, A. C.: High Earth-system climate sensitivity determined from
Pliocene carbon dioxide concentrations, *Nature Geoscience*, 3, 27-30, <https://doi.org/10.1038/ngeo724>, 2010.
- 490 Pan, L., Powell, E. M., Latychev, K., Mitrovica, J. X., Creveling, J. R., Gomez, N., ... and Clark, P. U.: Rapid
postglacial rebound amplifies global sea level rise following West Antarctic Ice Sheet collapse, *Science
Advances*, 7, eabf7787, <https://doi.org/10.1126/sciadv.abf7787>, 2021.
- 495 Pan, L., Milne, G. A., Latychev, K., Goldberg, S. L., Austermann, J., Hoggard, M. J., and Mitrovica, J. X.: The
influence of lateral Earth structure on inferences of global ice volume during the Last Glacial
Maximum, *Quaternary Science Reviews*, 290, 107644, <https://doi.org/10.1016/j.quascirev.2022.107644>,
2022.
- 500 Peltier, W. R.: The impulse response of a Maxwell Earth, *Reviews of Geophysics*, 12, 649-669,
<https://doi.org/10.1029/RG012i004p00649>, 1974.
- 505 Raymo, M. E., Mitrovica, J. X., O'Leary, M. J., DeConto, R. M., and Hearty, P. J.: Departures from eustasy in
Pliocene sea-level records, *Nature Geoscience*, 4, 328-332, <https://doi.org/10.1038/ngeo1118>, 2011.
- Richards, F. D., Coulson, S. L., Hoggard, M. J., Austermann, J., Dyer, B., and Mitrovica, J. X.: Geodynamically
corrected Pliocene shoreline elevations in Australia consistent with midrange projections of Antarctic ice
loss, *Science Advances*, 9, eadg3035, <https://doi.org/10.1126/sciadv.adg3035>, 2023.



- Rovere, A., Raymo, M. E., Mitrovica, J. X., Hearty, P. J., O'Leary, M. J., and Inglis, J. D.: The Mid-Pliocene sea-level conundrum: Glacial isostasy, eustasy and dynamic topography, *Earth and Planetary Science Letters*, 387, 27-33, <https://doi.org/10.1016/j.epsl.2013.10.030>, 2014.
- 510 Rowley, D. B., Forte, A. M., Moucha, R., Mitrovica, J. X., Simmons, N. A., and Grand, S. P.: Dynamic topography change of the eastern United States since 3 million years ago, *Science*, 340, 1560-1563. <https://doi.org/10.1126/science.1229180>, 2013.
- 515 Rohling, E. J., Foster, G. L., Grant, K. M., Marino, G., Roberts, A. P., Tamisiea, M. E., and Williams, F.: Sea-level and deep-sea-temperature variability over the past 5.3 million years, *Nature*, 508, 477-482, <https://doi.org/10.1038/nature13230>, 2014
- Sandstrom, M. R., O'Leary, M. J., Barham, M., Cai, Y., Rasbury, E. T., Wootton, K. M., and Raymo, M. E.: Age constraints on surface deformation recorded by fossil shorelines at Cape Range, Western
520 Australia, *Bulletin*, 133, 923-938, <https://doi.org/10.1130/B35564.1>, 2021.
- Sarnthein, M., Bartoli, G., Prange, M., Schmittner, A., Schneider, B., Weinelt, M., ... and Garbe-Schönberg, D.: Mid-Pliocene shifts in ocean overturning circulation and the onset of Quaternary-style climates, *Climate of the Past*, 5, 269-283, <https://doi.org/10.5194/cp-5-269-2009>, 2009.
525
- Siddall, M., Rohling, E. J., Thompson, W. G., and Waelbroeck, C.: Marine isotope stage 3 sea level fluctuations: Data synthesis and new outlook, *Reviews of Geophysics*, 46, <https://doi.org/10.1029/2007RG000226>, 2008.
- Sosdian, S., and Rosenthal, Y.: Deep-sea temperature and ice volume changes across the Pliocene-Pleistocene climate transitions, *Science*, 325, 306-310, <https://doi.org/10.1126/science.1169938>, 2009.
530
- Waelbroeck, C., Labeyrie, L., Michel, E., Duplessy, J. C., Mcmanus, J. F., Lambeck, K., ... and Labracherie, M.: Sea-level and deep water temperature changes derived from benthic foraminifera isotopic records, *Quaternary science reviews*, 21, 295-305, [https://doi.org/10.1016/S0277-3791\(01\)00101-9](https://doi.org/10.1016/S0277-3791(01)00101-9), 2002.
535
- Wardlaw, B. R., and Quinn, T. M.: The record of Pliocene sea-level change at Enewetak Atoll, *Quaternary Science Reviews*, 10, 247-258, [https://doi.org/10.1016/0277-3791\(91\)90023-N](https://doi.org/10.1016/0277-3791(91)90023-N), 1991.
- 540 Winnick, M. J., and Caves, J. K.: Oxygen isotope mass-balance constraints on Pliocene sea level and East Antarctic Ice Sheet stability, *Geology*, 43, 879-882, <https://doi.org/10.1130/G36999.1>, 2015
- Zachos, J., Pagani, M., Sloan, L., Thomas, E., and Billups, K.: Trends, rhythms, and aberrations in global climate 65 Ma to present, *Science*, 292, 686-693, <https://doi.org/10.1126/science.1059412>, 2001.